CLUSTER EXPLORATION USING INFORMATIVE MANIFOLD PROJECTIONS

A PREPRINT

Stavros Gerolymatos[1], **Xenophon Evangelopoulos**[2,3], **Vladimir Gusev**[1], **and John Y. Goulermas**[1]
[1]Department of Computer Science, University of Liverpool, Liverpool, England, UK
[2]Department of Chemistry, University of Liverpool, Liverpool, England, UK
[3]Leverhulme Research Centre for Functional Materials Design, University of Liverpool, England, UK
{s.gerolymatos, evangx, vladimir.gusev, j.y.goulermas}@liverpool.ac.uk

September 26, 2023

ABSTRACT

Dimensionality reduction (DR) is one of the key tools for the visual exploration of high-dimensional data and uncovering its cluster structure in two- or three-dimensional spaces. The vast majority of DR methods in the literature do not take into account any prior knowledge a practitioner may have regarding the dataset under consideration. We propose a novel method to generate informative embeddings which not only factor out the structure associated with different kinds of prior knowledge but also aim to reveal any remaining underlying structure. To achieve this, we employ a linear combination of two objectives: firstly, contrastive PCA that discounts the structure associated with the prior information, and secondly, kurtosis projection pursuit which ensures meaningful data separation in the obtained embeddings. We formulate this task as a manifold optimization problem and validate it empirically across a variety of datasets considering three distinct types of prior knowledge. Lastly, we provide an automated framework to perform iterative visual exploration of high-dimensional data.

1 Introduction

Data exploration focuses on identifying informative patterns to discover new insight and knowledge about a collection of data. The often high-dimensional nature of such data renders the visual exploration process intractable for the human eye, and therefore specialized data manipulation of the original samples is essential in practice. Dimensionality reduction methods have been at the forefront of this challenge Bishop [2006] aiming to recover lower-dimensional embeddings of the original data that facilitate the identification of underlying data cohorts and help understand better the problem at hand.

One of the most well known dimensionality reduction approaches perhaps is principal component analysis (PCA) Hotelling [1933], an efficient linear method aiming to maximizing the variance along the projection vectors, which in practice appears insufficient for meaningful separation of cohorts. A variety of non-linear methods have also been proposed that conversely focus on locally preserving the structure of the data such as Isomap Tenenbaum et al. [2000], LLE Roweis and Saul [2001], t-SNE van der Maaten and Hinton [2008], UMAP McInnes and Healy [2018], TriMap Amid and Warmuth [2019] and LargeVis Tang et al. [2016], etc. Projection pursuit (PP) Friedman and Tukey [1974], Caussinus and Ruiz-Gazen [2010] defines a family of dimensionality reduction methods that can enable various embedding effects depending on a suitably selected criterion. The kurtosis index Chiang et al. [2001] is one specific PP example that specializes in identifying "interesting" projections. Its minimization particularly penalizes the normality of the data distribution, promoting thus more meaningful separability when searching for clusters.

The above approaches nevertheless share the same attribute of offering a single static projection that does not consider any prior knowledge a practitioner may have regarding the high-dimensional latent structure. Such projections can be uninformative as they tend to illustrate the most evident features which are often already known by the reader. In practise, it has been shown Cavallo and Demiralp [2019] that an interactive or dynamic exploration of the available data can capture better their high-dimensional structure, especially when knowledge from a continual analysis of the

data or cohort distribution can be factored into the analysis. Recently, a number of such methods were introduced to dynamically generate new embeddings guided by the user Senanayake et al. [2019]. Sometimes, we want to obtain projections that remove variations with respect to some specific data samples. Contrastive PCA (cPCA) Abid et al. [2017] can be useful for this as it generates data projections which reveal structures that are more enriched in one data set relative to other data.

Our work focuses on computing informative data projections that factor out different types of prior knowledge and reveal any previously unknown high-dimensional structure. We achieved this by jointly minimizing a projection pursuit objective with a background variance-based objective. Here, prior knowledge reflects some information a practitioner has about the data and informativeness is interpreted as data separation which unveils unknown underlying structure.

Our method can be implemented on three different prior (background) knowledge cases. In each case, the prior knowledge is represented by a dataset whose structure we wish to remove from the obtained embeddings. More specifically, the cases are:

- **Attribute-based prior**. In this case, the prior data consist of a subset of attributes of the high-dimensional dataset. We want to obtain embeddings that reveal the structure associated with the remaining attributes by discounting the structure of the attributes of the prior dataset.
- **Sample-based prior**. We wish to visually explore a complex dataset that consists of the combination of a reference dataset (e.g. Fashion-MNIST) and a background dataset (e.g. MNIST). The background data modify and/or corrupt the reference dataset and we want to obtain embeddings that remove the background structure and disclose the reference one.
- **Subset-based prior**. The prior dataset consists of a subset of the original high-dimensional samples which are known to be similar to each other. By removing the structure associated with these samples, we can learn embeddings that reveal the structure of the remaining datapoints. Iterative visual exploration can take place in this setting by repeatedly updating the prior to include one of the clusters.

We specifically propose an efficient and effective optimization on the Stiefel manifold Stiefel [1935/36], which appears to empirically perform better compared to other related methods and helps circumvent numerical issues that are common in practice.

Our main contributions are as follows:

- A novel objective function which when optimised computes projections that factor out different types of prior knowledge while also revealing previously unknown underlying structure.
- Manifold optimisation modeling of the complex loss function to achieve numerical stability and fast convergence to a desirable solution.
- An iterative framework that can be applied to produce multiple informative projections for the visual data exploration of high-dimensional data.

The rest of the paper is organised as follows: Section 2 expands upon related literature and in Section 3 we give a detailed description of our proposed method. Section 4 provides a quantitative and qualitative analysis of our results and comparison with related approaches.

2 Related Work

A few works on interactive DR have been proposed in the last few years. Contrastive PCA Abid et al. [2017] computes data projections which highlight the salient structure of some reference data while discarding the structure of some background data. Conditional t-SNE (ct-SNE) Kang et al. [2021] is a generalisation of t-SNE which considers some prior knowledge in order to construct informative 2D embeddings. Prior knowledge corresponds to some information that the user is already aware of and can represented by a set of labels assigned to the data samples. The labels are either available before any analysis or can be inferred by clustering a set of embeddings. To discount the known factor of the labels, new embeddings are then generated which can provide insight on any underlying unknown structure. Unlike ct-SNE, which produces non-linear embeddings, SIDE Puolamäki et al. [2018] is a linear approach which takes as input some prior knowledge in terms of a background distribution of points. These points are known to be similar to each other either *a priori* or after some analysis. Projections that promote the maximal difference between the data and the background distribution are then computed. Another recently published method Puolamäki et al. [2021] allows a user to guide the examination procedure according to their own exploration interests. The users can formulate their prior knowledge as well as their specific interests in terms of relations among a subset of samples and a subset of attributes. These are then introduced to the model for computing the projections

Finding lower dimensional embeddings over matrix manifolds has recently become quite popular, mostly due to the flexibility the constraint-free manifold optimization offers Absil et al. [2007]. The (compact) Stiefel manifold Stiefel [1935/36], i.e., the set of all k-tuples of orthonormal vectors, has been employed in various dimensionality reduction applications Afsari and Krishnaprasad [2004], Theis et al. [2009], as well as in general machine learning ones Tompkins and Wolfe [2007], Cetingul and Vidal [2009]. More recently, the Grassmann manifold has been employed for lower dimensional embedding of 3D point clouds Haitman et al. [2021].

3 Methodology

In this section, we first exemplify the optimization details of our method. Secondly, we introduce our framework for structure extraction and knowledge update with which we can perform iterative visual exploration of high-dimensional data.

3.1 Objective formulation and Optimization

Let $\mathbf{X} \in \mathbb{R}^{n\times d}$ be the data matrix with each row $\{\mathbf{x}_i\}_{i=1}^n$ corresponding to the coordinates of the i^{th} data point. Our goal is to generate a set of low dimensional embedded points $\{\mathbf{q}_i\}_{i=1}^d \in \mathbb{R}^k$ (with $k \ll d$) that render meaningful data separation based on prior information to maximize data cohort informativeness.

Kurtosis Chiang et al. [2001] is a measure of non-normality that tends to reveal informative data cohorts within a dataset. For univariate data projections, the kurtosis is defined as:

$$\kappa = \frac{n\sum_{i=1}^{n}\left(\mathbf{v}^\top \mathbf{x}_i \mathbf{x}_i^T \mathbf{v}\right)^2}{\left(\mathbf{v}^\top \mathbf{X}^\top \mathbf{X}\mathbf{v}\right)^2} \tag{1}$$

where $\mathbf{v} \in \mathbb{R}^d$ is the projection vector.

We propose the combination of kurtosis and cPCA Abid et al. [2017] reconstruction loss term. cPCA can efficiently maintain areas of high-variance while discarding areas of no interest with low-variance. In our case, we wish to factor out from the projections areas which are associated with our prior knowledge. However, cPCA (as PCA) is not explicitly designed to provide low-dimensional projections that exhibit meaningful data segregation. As a result, it often happens that cPCA embeddings are not informative. By jointly optimizing kurtosis, improved data separation that can reveal underlying structure is ensured. Let us assume that $\{\mathbf{y}_i\}_{i=1}^m$ are some data associated with our prior knowledge.

We formulate the above requirements in the following optimization and term our proposed method as IMAPCE (Informative MAnifold Projections for Cluster Exploration) throughout the rest of the manuscript :

$$\begin{aligned}\mathbf{V}^\star = &\underset{\mathbf{V}\in\mathbb{R}^{d\times k}}{\arg\min}\, f(\mathbf{V}) \triangleq \|\mathbf{X} - \mathbf{X}\mathbf{V}\mathbf{V}^\top\|_F^2 - \alpha\|\mathbf{Y} - \mathbf{Y}\mathbf{V}\mathbf{V}^\top\|_F^2 + \\ &+ \mu n \sum_{i=1}^{n}\left[\mathbf{x}_i^\top \mathbf{V}(\mathbf{V}^\top\mathbf{X}^\top\mathbf{X}\mathbf{V})^{-1}\mathbf{V}^\top\mathbf{x}_i\right]^2 \\ &s.t.\quad \mathbf{V}^\top\mathbf{V} = \mathbf{I},\end{aligned} \tag{2}$$

where μ is a scaling parameter, α (as in cPCA) regulates the trade-off between having a high target variance and a low background data variance and $\mathbf{V} \in \mathbb{R}^{d\times k}$ with $k < d$ is the projection matrix to be computed. Setting $\alpha = 0$ corresponds to assuming no prior information (and therefore no prior data).

Due to its quartic form, the kurtosis index can have multiple local minima and thus its optimization is a challenging task. A set of quasi-power methods have recently emerged Hou and Wentzell [2011], Driscoll et al. [2019], Siyuan and Wentzell [2014] as a feasible and efficient alternative to gradient-based approaches. Nevertheless, they can be less stable when the covariance matrix $\mathbf{X}^\top\mathbf{X}$ is singular. To alleviate this issue a dimensionality reduction of the original samples, such as SVD is required and kurtosis is optimized on the newly embedded points and can often lead to weak representations.

To avoid this issue, we instead optimize Eq. (2) directly over the Stiefel manifold Stiefel [1935/36] $St(k,d) \triangleq \{\mathbf{M} \in \mathbb{R}^{d\times k} : \mathbf{M}^\top\mathbf{M} = \mathbf{I}\}$ which is a subset of the Euclidean space $\mathbb{R}^{d\times k}$. The optimization can be carried out using any gradient-based solver, such as steepest decent Absil et al. [2007] for example, without the need to perform any preprocessing on the original data due to singularity issues.

The gradient of $f(\mathbf{V})$ is given as

$$\begin{aligned}\nabla_{\mathbf{V}} f(\mathbf{V}) = 2\big(\alpha \mathbf{Y}^\top \mathbf{Y} - \mathbf{X}^\top \mathbf{X}\big)\mathbf{V} \\ + 4\mu n \sum_{i=1}^{n-m} \big(\mathbf{x}_i^\top \mathbf{V}\mathbf{A}^{-1}\mathbf{V}^\top \mathbf{x}_i\big)\big[(\mathbf{x}_i\mathbf{x}_i^\top)\mathbf{V}\mathbf{A}^{-1} \\ - \big(\mathbf{X}^\top \mathbf{X}\big)\mathbf{V}\mathbf{A}^{-1}\big(\mathbf{V}^\top \mathbf{x}_i\mathbf{x}_i^\top \mathbf{V}\big)\mathbf{A}^{-1}\big],\end{aligned} \tag{3}$$

where $\mathbf{A} = \mathbf{V}^\top \mathbf{X}^\top \mathbf{X}\mathbf{V}$. For visualization purposes we usually set $k = 2, 3$ and in practice therefore $\mathbf{A} \in \mathbb{R}^{k\times k}$ is of small size, rendering its condition number $\kappa(\mathbf{A}) = ||\mathbf{A}||_F / ||\mathbf{A}^{-1}||_F$ to be relatively small and well-conditioned. By jointly minimizing both objectives of Eq. (2) on the Stiefel manifold we avoid any singularity issues and at the same time obtain more informative separability of cohorts as we will empirically demonstrate later in the experiments.

IMAPCE has a limitation that derives from the optimisation of kurtosis. More specifically, minimisation of kurtosis was found to produce cluster artifacts for datasets whose size was very close to their dimensionality Hou and Wentzell [2011]. As a result, the same holds for IMAPCE and preprocessing (e.g. PCA or SVD) is essential for such datasets.

3.2 Iterative Visual Exploration

In the case of a subset-based prior, we are *a priori* aware that a subset of samples of some high-dimensional data are similar to each other (e.g. they share the same class) and we wish to explore the cluster structure of the remaining data points. To achieve this, we calculate and optimise the kurtosis term over the remaining (subset of unexplored) samples which are defined as $\{\mathbf{z}_i\}_{i=1}^{(n-m)} = \{\mathbf{x}_i\}_{i=1}^{n} \backslash \{\mathbf{y}_i\}_{i=1}^{m}$. As a result, the obtained projections provide meaningful data separation of the unexplored samples and reveal their cluster structure.

To extract the structure of the unexplored samples $\mathbf{Z}$, we perform the clustering of their embeddings. While the obtained clusters unveil some previously unknown structure, some of them are not as informative as others. We argue that the cluster which is the most separated from the rest, is the most informative and refer to it as the *most distinct*. We extract this cluster because it is expected to have the greatest probability of consisting of very similar points. Subsequently, we dynamically update our prior data $\mathbf{Y}$ to include the points of this cluster, while also removing them from the unexplored subset $\mathbf{Z}$. Optimisation of Eq. (2) takes then place to compute new 2D embeddings that exhibit data separation of the updated unexplored data where cluster extraction can again be performed. This process continues iteratively until no more data remain unexplored and can efficiently provide gradual exploration of the unknown underlying structure of high-dimensional data.

To cluster the embeddings we used the Bayesian infinite Gaussian mixture model Rasmussen [1999], Anderson [1991], Neal [2000], commonly referred to as Dirichlet Process Gaussian Mixture Model (DPGMM) as it does not require a predefined number of clusters (but rather a maximum cluster number) and due to its performance quality. More information about the DPGMM is provided in the Dirichlet Process Gaussian Mixture Model Appendix.

Given the mean $\mathbf{m}_l$ and covariance matrix $\mathbf{C}_l$ for each cluster l, we can extract the most distinct cluster by calculating all pairwise distances of cluster centers and their respecive distributions using the Mahalanobis distance Mahalanobis [1936]

$$\delta_{lj} = \sqrt{(\mathbf{m}_j - \mathbf{m}_l)^\top \mathbf{C}_l^{-1}(\mathbf{m}_j - \mathbf{m}_l)}. \tag{4}$$

To avoid selecting a small deal of outliers as a cluster, we define a minimum acceptable cluster size. All clusters with number of points less than that are discarded as outliers and their distances are not considered. From Eq. (4) we define a symmetric pairwise distances matrix for all clusters as $D_{lj} = (\delta_{lj} + \delta_{jl})/2$ and the most distinct cluster is given by

$$c^\star = \arg\max \mathbf{D}\mathbf{1}, \tag{5}$$

where $\mathbf{1}$ is the vector of all ones. As a special case, if only two clusters of acceptable size are detected, then both are chosen as most distinct. Algorithm 1 outlines the major steps of our proposed iterative framework.

3.3 Hyperparameter tuning

Hyperparamaters α and μ have to be chosen for IMAPCE. We need to select α if there are prior data (otherwise it is set to zero), while μ has to be selected regardless of the availabilty of prior data. As a rule of thumb, setting $\alpha = 1$ empirically provides embeddings with a desirable trade-off between high original data variance and low prior data variance. In practise we observe that the kurtosis term is not greater than 10-20. After computing the cPCA (PCA if

Algorithm 1 Iterative Visual Exploration

Input: original data $\{\mathbf{x}_i\}_{i=1}^{n}$, prior data $\{\mathbf{y}_i\}_{i=1}^{m}$, unexplored data $\{\mathbf{z}_i\}_{i=1}^{n-m}$, acceptable cluster size s (for termination criterion)
Output: Embeddings $\mathbf{Q}$.

while $(n-m) > s$ **do**
  $\mathbf{V}^\star = \underset{\mathbf{V} \in St(k,d)}{\arg\min}\ f(\mathbf{V})$
  $\mathbf{Q} = \mathbf{Z}\mathbf{V}^\star$ {Embeddings of unexplored data}
  $\{\mathbf{m}\}_l^r, \{\mathbf{C}\}_l^r \sim DPGMM\big(\{\mathbf{q}_i\}_{i=1}^{n-m}\big)$ {Clustering}
  for all cluster pairs (l, j) **do**
    $\delta_{lj} = \sqrt{(\mathbf{m}_j - \mathbf{m}_l)^\top \mathbf{C}_l^{-1} (\mathbf{m}_j - \mathbf{m}_l)}$
    $D_{lj} = (\delta_{lj} + \delta_{jl})/2$
  end for
  $c^\star = \arg\max \mathbf{D1}$ {Most distinct cluster calculation}
  $\mathbf{X}_c = \{\mathbf{x} : \mathbf{x} \in c^\star\}$ {Points of most distinct cluster}
  $\mathbf{Y} = \mathbf{Y} \cup \mathbf{X}_c$ {Update of prior data and their size m}
  $\mathbf{Z} = \mathbf{Z} \backslash \mathbf{X}_c$ {Update of unexplored data}
end while

there are no prior data) reconstruction error of our original data, μ is selected as one or two orders of magnitude below the cPCA reconstruction error. In this way, kurtosis can influence the optimization. As for s which needs to be selected for the iterative visual exploration, it denotes the minimum acceptable size of a cluster and is used for discarding outliers as well as stopping the exploration process. Its choice depends on the size and dimensionality of the original data.

4 Experimental Setup

To showcase that IMAPCE can efficiently factor out different types of prior knowledge, we ran experiments on several datasets for all previously mentioned prior knowledge types. We provide both quantitative and qualitative results and compare the performance of IMAPCE with cPCA and ct-SNE. We compare with them because they have the same goal with IMAPCE, which is to generate embeddings that promote some underlying structure of the data while removing any prior knowledge.

For cPCA, a few projection matrices are computed for a fixed user-selected number of α's (trade-off hyperparameter) and spectral clustering is applied to them. The projection matrix which corresponds to the cluster medoid is used to compute the projections. For ct-SNE, the label information which we wish to remove from the embeddings is given as prior data. Details about its hyperparameters' selection are provided for each dataset.

We implemented our method on Python and used Pymanopt Townsend et al. [2016] which is a Python toolbox for optimization on Riemannian manifolds. The DPGMM used for clustering is implemented via the Sci-kit learn library of Python Pedregosa et al. [2011]. IMAPCE and cPCA implementations are given in `https://github.com/StavGer/IMAPCE` , while for ct-SNE we used the official implementation. We present the experimental section in a prior-wise manner.

4.1 Attribute-based prior

The task in this case is to generate embeddings that factor out the structure of one or more selected attributes of the high-dimensional data in order to reveal the structure of the remaining attributes. We ran experiments using IMAPCE, ct-SNE and cPCA and compare their performance on both synthetic and real-world data.

4.1.1 Synthetic data

The synthetic dataset Heiter et al. [2023] consists of 1500 ten-dimensional points. All points are assigned to one of two clusters (with centers sampled from $\mathcal{N}(0, 25)$) in the first four dimensions and one of three clusters (with centers sampled from $\mathcal{N}(0, 1)$) in dimensions 5-6. For each point we add noise from $\mathcal{N}(0, 0.01)$. The last four dimensions correspond to samples from $\mathcal{N}(0, 1)$. To run IMAPCE (we set $\alpha = 1$, $\mu = 200$) and cPCA, we define as prior data the first four dimensions and wish to generate embeddings that reveal the complementary cluster structure of dimensions

5-6. With the same goal, we implement ct-SNE (by selecting its hyperparameters according to Heiter et al. [2023]) using the cluster labels of the first four dimensions as prior knowledge.

The generated embeddings are visualised in figures 1(a)-1(c) where prior data information is encoded according to shape and complementary structure according to color. We observe that cPCA embeddings are clustered with respect to their shape, indicating that the structure of prior data is not removed. On the contrary, both ct-SNE and IMAPCE compute embeddings that factor out the prior information as there is mix of points with different shapes. However, ct-SNE fails to reveal the complementary cluster structure since embeddings with different colors are mixed. On the other hand, IMAPCE clearly groups the embeddings according to their colors, unveiling the complementary structure.

The normalised Laplacian score was proposed Kang et al. [2021] in order to quantify the presence of some prior label information on a set of embeddings. This score takes values in [0, 1] and measures the label homogeneity within a user-selected neighborhood in an embedding set. If the embeddings remove the structure associated with some prior data labels, we expect the Laplacian to be large when computed with respect to these labels.

To quantitatively compare how well cPCA, ct-SNE and IMAPCE embeddings factor out the prior information, we calculated the Laplacian scores on the prior information of dimensions 1-4. We provide the scores for a range of different neighborhood sizes (hyperparameter of Laplacian score) in Figure 1(d). IMAPCE achieved higher Laplacian scores (lower homogeneity) than cPCA and ct-SNE, indicating that it removes the prior information more effectively than them (as was observed qualitatively). Given that the kurtosis term makes the difference between cPCA and IMAPCE, we can infer that its inclusion in IMAPCE achieves the meaningful data separation that reveals some unknown structure which is missed by cPCA.

4.1.2 UCI Adult data

We sampled 1000 data points from the UCI Adult dataset Becker and Kohavi [1996] which consists of six features. Age, education level, and work hours per week are numeric ones while ethnicity (white/other), gender (male/female) and income ($>$ 50k) are binary ones.

Using the ethnicity feature as prior, we obtain cPCA, ct-SNE (selecting its hyperparameters according to the original work Kang et al. [2021]) and IMAPCE ($\alpha = 1, \mu = 150$) embeddings as shown in figures 1(e) - 1(g). cPCA provides embeddings with mixed ethnicity, gender and income features, failing to exhibit any clear cluster formation. On the contrary, ct-SNE contains clusters of different gender and income points but does not remove the prior information as there are also clusters of different ethnicites. Finally, IMAPCE embeddings remove the prior information by having mixed ethnicities while they also reveal the cluster structure of both gender (red-green colors) and income (filled-unfilled markers) attributes.

Similar to the synthetic data experiments, we compared the Laplacian scores of cPCA, ct-SNE and IMAPCE embeddings evaluated on the ethnicity prior as shown in Figure 1(h). IMAPCE has larger Laplacian scores and thus discounts the ethnicity prior information more effectively than both cPCA and ct-SNE. Equivalent experiments using gender attribute as well as the combination of gender and income attributes as priors are provided in the UCI Adult Data Embeddings Appendix.

4.2 Sample-based prior

We created some complex data by combining instances from MNIST (which we consider as background data) and Fashion-MNIST (which we consider as reference data) datasets. The task in this case is to compute two-dimensional embeddings of complex data that remove the information associated with the MNIST data and provide separation according to the complementary structure defined by the Fashion-MNIST labels.

We construct a series of complex data (6000 samples each) by choosing samples from two-specific Fashion-MNIST ground truth classes and superimposing them with randomly selected MNIST instances, as shown in figure 1(i). The superimposed 28x28 images, as well as the MNIST images serving as the background, are flattened to 784 dimensional vectors before their processing. As background data we select 1000 MNIST samples which are not necessarily used when constructing the complex data. While we can employ these prior data for both IMAPCE and cPCA, ct-SNE is limited to label priors. To remove the MNIST information using ct-SNE, we provide it with the ground truth labels of the MNIST instances that were used for the complex data construction. We selected its hyperparameters according to the suggestions of the authors. Finally, for IMAPCE we set $\alpha = 1$ and $\mu = 10^5$.

Figures 1(j)-1(l) show complex data embeddings (with 'Bag', 'Ankle-boot' Fashion MNIST ground truth labels) generated by IMAPCE, cPCA and ct-SNE. We observe that ct-SNE completely fails to separate the embeddings according to their Fashion-MNIST class. While cPCA factors out to some extent the MNIST structure, its embeddings exhibit significant overlap in terms of their Fashion-MNIST classes. IMAPCE computes embeddings that effectively

remove the MNIST information and thus achieve the clearest separation with respect to their Fashion-MNIST class. Therefore, optimisation of kurtosis term provides enhanced and interpretable data segregation which is not achieved by cPCA.

To verify our observations, we trained and tested an SVM classifier (75% training, 25% test) on the classification of the calculated 2D embeddings with respect to their Fashion-MNIST labels. By doing this, we can quantify the separability according to the complementary structure which we wish to unveil. The test-set accuracy is averaged over 10 random train-test splits and given in Table 1. The very poor performance of the ct-SNE embeddings as well as the superior performance achieved by the IMAPCE ones confirm our observations. Experiments for a few more complex data are given in the Complex Data Embeddings Appendix.

Method	Accuracy
cPCA	0.78 ± 0.007
ct-SNE	0.10 ± 0.006
IMAPCE	$\mathbf{0.98} \pm 0.003$

Table 1: Accuracy scores for SVM classification on the 2D embeddings of IMAPCE, cPCA and ct-SNE.

4.3 Subset-based prior

In this setup, prior data are subsets of the original data that share the same class (and are thus similar). The goal is to generate embeddings that reveal the cluster structure of the remaining samples (unexplored subset) within these datasets. By employing our structure extraction framework with IMAPCE or cPCA, we can dynamically update the prior data after each set of embeddings. As a result, we sequentially obtain new sets of informative embeddings that gradually unveil the underlying cluster structure of all high-dimensional data. In this case, we did not compare with ct-SNE because the prior data are subsets of the original data. Thus, it is non-trivial to define some cluster labels for all high-dimensional samples (which is essential for ct-SNE).

We performed the iterative visual exploration of Image Segmentation data from the UCI machine learning repository Dua and Graff [2017] under various prior data assumptions. This dataset consists of 2310 samples and 19 attributes and includes 330 instances from 7 different classes, namely "sky", "grass", "path", "foliage", "cement", "brickface", "window".

Assuming no prior data and selecting $\alpha = 1$, $\mu = 10^5$, $s = 75$, we sequentially implement IMAPCE on UCI Image segmentation data. The obtained projections are shown in Figure 2, where each subfigure consists of three subplots. The upper subplot illustrates the IMAPCE data projections for a specific iteration of the process. Grey points correspond to the prior data, while black points correspond to the unexplored subset of samples. The middle plot shows the results of a DPGMM clustering on the unexplored points where the most distinct cluster is marked with a black frame. The lower subplot shows the unexplored points coloured according to their ground truth class.

The first data projection is shown in Figure 2(a). The upper plot consists of solely black points as there are no prior data. All data are clustered in the middle subplot and the green cluster is the most distinct. Its points are considered very similar and are stored for the evaluation stage. Subsequently, these points define the prior data and are removed from the unexplored data. Afterwards, the second iteration takes place and new informative embeddings are calculated and shown in Figure 2(b). Separation of data samples that were previously overlapping is now observed and indicative of an informative data projection. The grey points of the upper subplot correspond to the prior data while the black ones refer to the unexplored points. The unexplored points are clustered in the middle subplot and blue is the most distinct cluster. Its points are then incorporated in the prior data while removed from the unexplored data.

This iterative process is repeated until no clusters are formed (only outliers are left). Gradual exploration of the whole dataset contributes to the extraction of new and meaningful underlying structure. For brevity and demonstration reasons, the rest of the exploration analysis is omitted while the first four iterations are illustrated in Figures 2(a)-2(d).

To quantitatively compare IMAPCE and cPCA, we ran several experiments on UCI Image Segmentation ($\alpha = 1$, $\mu = 10^5$, $s = 75$) with different initial subsets of prior data. Performance evaluation took place after the exploration of a dataset has finished. During the evaluation stage, the quality of the most distinct clusters (which are stored along the exploration process) is measured with respect to their ground truth labels using the Jaccard Jaccard [1901] and NMI scores. Both scores are highly used in the literature for the evaluation of clusters' quality. Detailed results for IMAPCE and cPCA are given in Table 2. We consider the case of no prior data, while we also experiment by setting as prior subsets, data samples from every ground truth class.

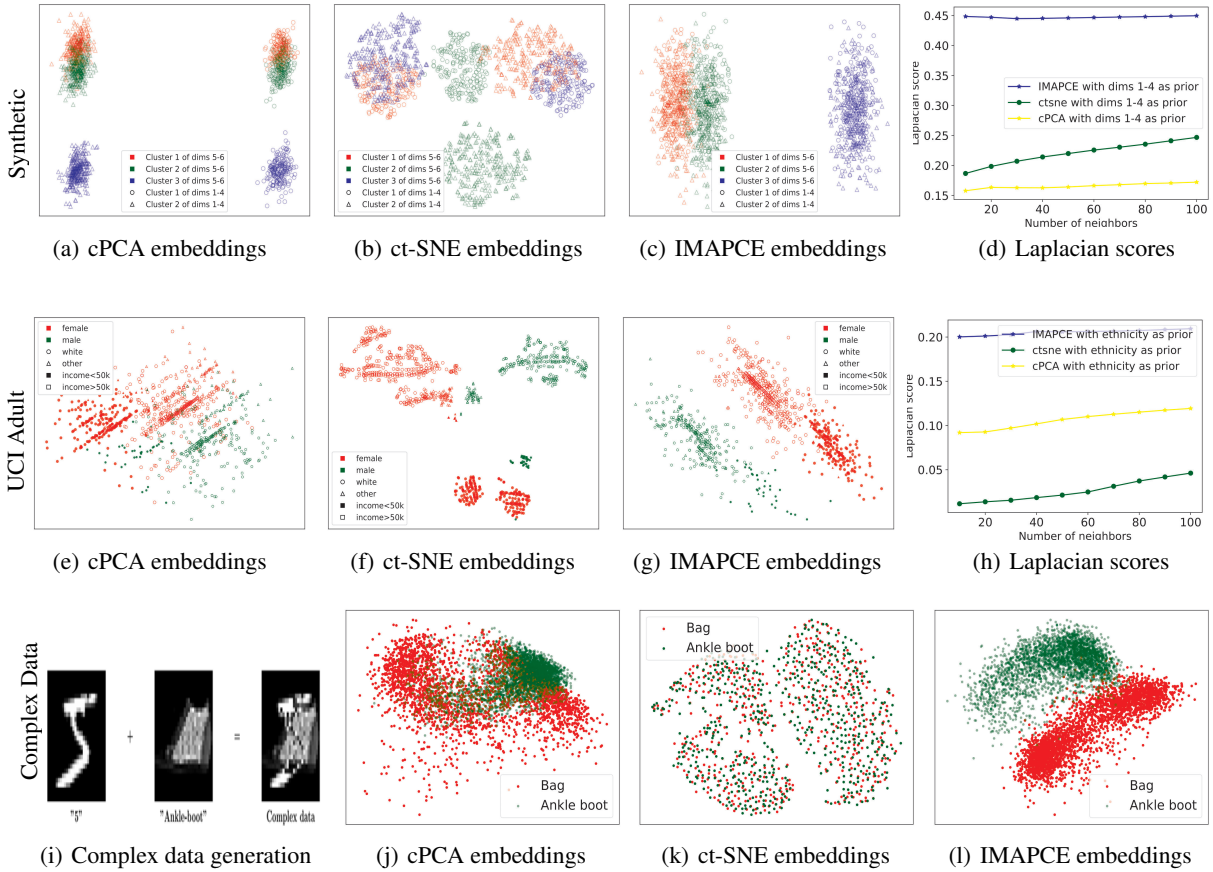

(a) cPCA embeddings (b) ct-SNE embeddings (c) IMAPCE embeddings (d) Laplacian scores

(e) cPCA embeddings (f) ct-SNE embeddings (g) IMAPCE embeddings (h) Laplacian scores

(i) Complex data generation (j) cPCA embeddings (k) ct-SNE embeddings (l) IMAPCE embeddings

Figure 1: Top row shows synthetic data experiments with information of dimensions 1-4 as prior. Middle row illustrates UCI adult data experiments with ethnicity feature as prior. Bottom row shows complex data experiments using MNIST data as prior. (a) cPCA embeddings are clusterred w.r.t. dimensions 1-4 labels. (b) ct-SNE embeddings are mixed w.r.t. labels of dimensions 1-4 but not clustered w.r.t labels of dimensions 5-6 (complementary structure). (c) IMAPCE embeddings are clustered w.r.t. labels of dimensions 5-6 (with mixed labels of dimensions 1-4). (d) Laplacian scores for synthetic embeddings using labels of dimensions 1-4. (e) cPCA embeddings have mixed ethnicity, gender and income labels. (f) ct-SNE clusters w.r.t. gender and income and ethnicity. (g) IMAPCE clusters w.r.t. gender and income (revealing complementary structure). (h) Laplacian scores for UCI adult embeddings using ethnicity labels. (i) Complex data generation. (j) cPCA embeddings highly overlap w.r.t. to their Fashion-MNIST class. (k) ct-SNE embeddings are completely mixed w.r.t. to their Fashion-MNIST class. (l) IMAPCE embeddings exhibit clear segregation w.r.t. Fashion-MNIST class.

Overall, IMAPCE clearly outperforms cPCA on both scores under all prior data assumptions. The superior Jaccard and NMI scores of IMAPCE indicate that it promotes enhanced cluster segregation in comparison to cPCA. This is achieved due to the optimisation of the kurtosis term. We provide equivalent quantitative results for 10000 randomly selected MNIST instances in the Iterative Exploration of MNIST appendix.

5 Conclusion

To sum up, in this work we proposed IMAPCE to generate low-dimensional embeddings that filter out three different types of prior knowledge while also revealing any previously unknown underlying structure. To ensure numerical stability and fast convergence, we performed the optimisation over the Stiefel manifold. Additionally, we introduced an iterative framework that can be employed with IMAPCE to sequentially compute multiple embeddings of high-dimensional data. Finally, we ran experiments on diverse datasets for different prior knowledge types and provided both quantitative and qualitative results as well as comparisons with related approaches.

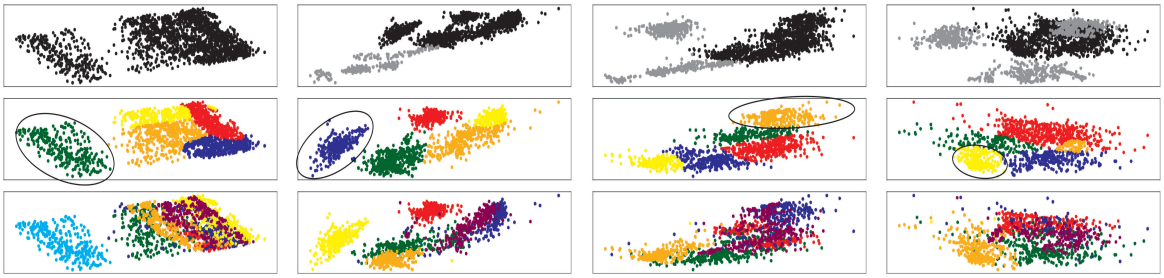

(a) (b) (c) (d)

Figure 2: Iterative exploration of UCI image segmentation data by IMAPCE. Each triplet of subfigures corresponds to an iteration of the exploration process. In every triplet: The upper plot shows the data projections where prior data are colored in grey while the unexplored subset in black, The middle plot shows the clustering of the unexplored points according to a DPGMM and the most distinct cluster in a black frame, The bottom plot illustrates the unexplored points colored according to their ground truth label.

Method	Prior data class	Mean Jaccard Score	NMI
cPCA Abid et al. [2017]	-	0.44	0.46
IMAPCE	-	$\mathbf{0.63} \pm 0.05$	$\mathbf{0.67} \pm 0.06$
cPCA Abid et al. [2017]	Brickface	0.49	0.6
IMAPCE	Brickface	$\mathbf{0.63} \pm 0.04$	$\mathbf{0.67} \pm 0.06$
cPCA Abid et al. [2017]	Cement	0.47	0.6
IMAPCE	Cement	$\mathbf{0.64} \pm 0.07$	$\mathbf{0.69} \pm 0.06$
cPCA Abid et al. [2017]	Foliage	0.47	0.61
IMAPCE	Foliage	$\mathbf{0.65} \pm 0.05$	$\mathbf{0.72} \pm 0.05$
cPCA Abid et al. [2017]	Grass	0.5	0.48
IMAPCE	Grass	$\mathbf{0.59} \pm 0.08$	$\mathbf{0.64} \pm 0.08$
cPCA Abid et al. [2017]	Window	0.5	0.57
IMAPCE	Window	$\mathbf{0.68} \pm 0.06$	$\mathbf{0.74} \pm 0.04$
cPCA Abid et al. [2017]	Sky	0.35	0.43
IMAPCE	Sky	$\mathbf{0.57} \pm 0.05$	$\mathbf{0.61} \pm 0.07$
cPCA Abid et al. [2017]	Path	0.43	0.56
IMAPCE	Path	$\mathbf{0.59} \pm 0.06$	$\mathbf{0.65} \pm 0.07$

Table 2: Jaccard (averaged over all classes) and NMI scores for the evaluation of IMAPCE and cPCA on the visual exploration of the UCI Image Segmentation data under different prior data assumptions. Ten random initialisations were used for IMAPCE.

6 Acknowledgments

Xenophon Evangelopoulos acknowledges financial support from the Leverhulme Trust via the Leverhulme Research Centre for Functional Materials Design.

The work was also supported by a studentship from the School of Electrical Engineering, Electronics and Computer Science, at the University of Liverpool, UK.

References

Christopher M. Bishop. *Pattern Recognition and Machine Learning (Information Science and Statistics)*. Springer-Verlag, 2006. ISBN 0387310738.

Harold Hotelling. Analysis of a complex of statistical variables into principal components. *Journal of Educational Psychology*, 24:498–520, 1933.

Joshua B. Tenenbaum, Vin de Silva, and John C. Langford. A global geometric framework for nonlinear dimensionality reduction. *Science*, 290(5500):2319, 2000.

Sam Roweis and Lawrence Saul. Nonlinear dimensionality reduction by locally linear embedding. *Science (New York, N.Y.)*, 290:2323–6, 2001.

Laurens van der Maaten and Geoffrey Hinton. Visualizing data using t-sne. *Journal of Machine Learning Research*, 9 (86):2579–2605, 2008.

Leland McInnes and John Healy. Umap: Uniform manifold approximation and projection for dimension reduction. *ArXiv*, abs/1802.03426, 2018.

Ehsan Amid and Manfred K. Warmuth. TriMap: Large-scale Dimensionality Reduction Using Triplets. *arXiv preprint arXiv:1910.00204*, 2019.

Jian Tang, Jingzhou Liu, Ming Zhang, and Qiaozhu Mei. Visualizing large-scale and high-dimensional data. In *Proceedings of the 25th International Conference on World Wide Web*. International World Wide Web Conferences Steering Committee, apr 2016.

Jerome Friedman and J.W. Tukey. A projection pursuit algorithm for exploratory data analysis," ieee transactions on computers, c-23, 881-889. *Computers, IEEE Transactions on*, C 23:881 – 890, 10 1974.

Henri Caussinus and Anne Ruiz-Gazen. *Exploratory Projection Pursuit*, volume 82, pages 67 – 92. 01 2010. ISBN 9780470611777.

S.-S. Chiang, C.-I. Chang, and I.W. Ginsberg. Unsupervised target detection in hyperspectral images using projection pursuit. *IEEE Transactions on Geoscience and Remote Sensing*, 39(7):1380–1391, 2001.

Marco Cavallo and Çağatay Demiralp. Clustrophile 2: Guided visual clustering analysis. *IEEE Transactions on Visualization and Computer Graphics*, 25(1):267–276, 2019. ISSN 1077-2626.

Damith A. Senanayake, Wei Wang, Shalin H. Naik, and Saman K. Halgamuge. Self-organizing nebulous growths for robust and incremental data visualization. *IEEE Transactions on Neural Networks and Learning Systems*, 32: 4588–4602, 2019.

Abubakar Abid, Vivek Kumar Bagaria, Martin Zhang, and James Zou. Contrastive principal component analysis. 09 2017.

Edward Stiefel. Richtungsfelder und fernparallelismus in n-dimensionalen mannigfaltigkeiten. *Commentarii mathematici Helvetici*, 8:305–353, 1935/36.

Bo Kang, Darío García García, Jefrey Lijffijt, Raúl Santos-Rodríguez, and Tijl de Bie. Conditional t-sne: More informative t-sne embeddings. In *2021 IEEE 8th International Conference on Data Science and Advanced Analytics (DSAA)*, pages 1–2, 2021.

Kai Puolamäki, Emilia Oikarinen, Bo Kang, Jefrey Lijffijt, and Tijl De Bie. Interactive visual data exploration with subjective feedback: An information-theoretic approach. In *2018 IEEE 34th International Conference on Data Engineering (ICDE)*, pages 1208–1211, 2018.

Kai Puolamäki, Emilia Oikarinen, and Andreas Henelius. Guided visual exploration of relations in data sets. *Journal of Machine Learning Research*, 22(96):1–32, 2021.

P.-A. Absil, Robert Mahony, and Rodolphe Sepulchre. *Optimization Algorithms on Matrix Manifolds*. Princeton University Press, 2007. ISBN 0691132984.

Bijan Afsari and Perinkulam S Krishnaprasad. Some gradient based joint diagonalization methods for ica. In *Independent Component Analysis and Blind Signal Separation: Fifth International Conference, ICA 2004, Granada, Spain, September 22-24, 2004. Proceedings 5*, pages 437–444. Springer, 2004.

Fabian J. Theis, Thomas P. Cason, and P. A. Absil. Soft dimension reduction for ica by joint diagonalization on the stiefel manifold. In Tülay Adali, Christian Jutten, João Marcos Travassos Romano, and Allan Kardec Barros, editors, *Independent Component Analysis and Signal Separation*, pages 354–361. Springer Berlin Heidelberg, 2009.

Frank Tompkins and Patrick J Wolfe. Bayesian filtering on the stiefel manifold. In *2007 2nd IEEE International Workshop on Computational Advances in Multi-Sensor Adaptive Processing*, pages 261–264. IEEE, 2007.

Hasan Ertan Cetingul and René Vidal. Intrinsic mean shift for clustering on stiefel and grassmann manifolds. In *2009 IEEE Conference on Computer Vision and Pattern Recognition*, pages 1896–1902. IEEE, 2009.

Yuval Haitman, Joseph M. Francos, and Louis L. Scharf. Grassmannian dimensionality reduction for optimized universal manifold embedding representation of 3d point clouds. In *2021 IEEE/CVF International Conference on Computer Vision Workshops (ICCVW)*, pages 4196–4204, 2021.

Siyuan Hou and Peter Wentzell. Fast and simple methods for the optimization of kurtosis used as a projection pursuit index. *Analytica chimica acta*, 704:1–15, 2011.

Steve Driscoll, Yannick MacMillan, and Peter Wentzell. Sparse projection pursuit analysis: An alternative for exploring multivariate chemical data. *Analytical Chemistry*, 12 2019.

Hou Siyuan and Peter Wentzell. Re-centered kurtosis as a projection pursuit index for multivariate data analysis. *Journal of Chemometrics*, 28, 2014.

Carl Edward Rasmussen. The infinite gaussian mixture model. In *Proceedings of the 12th International Conference on Neural Information Processing Systems*, NIPS'99, page 554–560. MIT Press, 1999.

John R. Anderson. The adaptive nature of human categorization. *Psychological Review*, 98(3):409–429, 1991.

Radford M. Neal. Markov chain sampling methods for dirichlet process mixture models. *Journal of Computational and Graphical Statistics*, 9:249 – 265, 2000.

Prasanta Chandra Mahalanobis. On the generalized distance in statistics. *Proceedings of the National Institute of Sciences (Calcutta)*, 2:49–55, 1936.

James Townsend, Niklas Koep, and Sebastian Weichwald. Pymanopt: A python toolbox for optimization on manifolds using automatic differentiation. *Journal of Machine Learning Research*, 17(137):1–5, 2016.

F. Pedregosa, G. Varoquaux, A. Gramfort, V. Michel, B. Thirion, O. Grisel, M. Blondel, P. Prettenhofer, R. Weiss, V. Dubourg, J. Vanderplas, A. Passos, D. Cournapeau, M. Brucher, M. Perrot, and E. Duchesnay. Scikit-learn: Machine learning in Python. *Journal of Machine Learning Research*, 12:2825–2830, 2011.

Edith Heiter, Bo Kang, Ruth Seurinck, and Jefrey Lijffijt. Revised conditional t-sne: Looking beyond the nearest neighbors. In *Advances in Intelligent Data Analysis XXI*, page TBD, Cham, 2023. Springer International Publishing.

Barry Becker and Ronny Kohavi. Adult. UCI Machine Learning Repository, 1996. DOI: https://doi.org/10.24432/C5XW20.

Dheeru Dua and Casey Graff. UCI machine learning repository, 2017.

Paul Jaccard. Distribution de la flore alpine dans le bassin des dranses et dans quelques régions voisines. *Bulletin de la Societe Vaudoise des Sciences Naturelles*, 37:241–72, 01 1901.

A Dirichlet Process Gaussian Mixture Model

A Gaussian mixture model with K components can be described by

$$p(\mathbf{z}|\{\theta_l\}_{l=1}^{K}) = \sum_{l=1}^{K} \mathbf{w}_l \mathcal{N}(\mathbf{z}|\mathbf{m}_l, \mathbf{C}_l^{-1}), \tag{6}$$

where $\theta_l = \{\mathbf{w}_l, \mathbf{m}_l, \mathbf{C}_l^{-1}\}$ is the set of parameters for component l, $\mathbf{w}_l$ are the mixing weights of the Gaussians (or clusters here) satisfying $\sum_{i=l}^{K} \mathbf{w}_l = 1$, $\mathbf{m}_l$ is the mean vector for cluster l, and $\mathbf{C}_l^{-1}$ is its inverse covariance matrix. The latter ones are modeled by a joint Normal/Wishart distribution

$$(\mathbf{m}_l, \mathbf{C}_l^{-1}) \sim \mathcal{NW}(\xi, \rho, \beta, W) \tag{7}$$

Here, ξ corresponds to a prior of the mean of cluster l, $\mathbf{m}_l$, ρ is a scalar representing how strongly we believe this prior. $\mathbf{W}$ is a prior of the precision (inverse Covariance matrix) matrix of cluster l, $\mathbf{C}_l^{-1}$ and β represents how strongly we believe this prior. The DPGMM model follows a hierarchical structure where the data is modeled first as in eq. (6), then the component parameters and finally the various hyperparameters of those Rasmussen [1999].

B UCI Adult Data Embeddings

Using the gender attribute as prior, we obtain embeddings for cPCA, ct-SNE and IMAPCE as shown in Figures 3(a)-3(c). cPCA embeddings are mixed in terms of ethnicities, gender and income. However, they do not exhibit any cluster structure. On the other hand, ct-SNE embeddings have mixed genders (and thus they remove the prior knowledge) and are clustered according to income (filled and unfilled markers) as well as ethnicity (circles and triangles). IMAPCE embeddings are mixed in terms of gender (factoring out the prior information) while they also reveal the complementary structure as they provide clear separation with respect to income and also some separation with respect to ethnicity (triangles are mostly located on the upper part). Laplacian scores are calculated for all embeddings using the gender labels and are shown for a range of neighborhood sizes in figure 3(d). IMAPCE embeddings achieve slightly higher Laplacian scores (lower homogeneity) than ct-SNE ones, which means that IMAPCE discounts the prior information a bit more effectively. On the contrary, cPCA embeddings fail to remove the prior knowledge as they are associated with very low Laplacian scores.

Using the combination of gender and ethnicity features as prior, we compute embeddings of cPCA, ct-SNE and IMAPCE and visualise them in Figures 3(e)-3(g). We observe that cPCA produces the same uninformative set of embeddings regardless of the selection of the prior attribute. ct-SNE embeddings are clustered according to their income attribute and their clusters consist of mixed gender and ethnicity points. Similar observations can be made for the IMAPCE embeddings. Figure 3(h) illustrates the Laplacian scores computed with respect to the combination of gender and ethnicity labels. IMAPCE filters out the prior information slightly better than ct-SNE in this case as well.

C Complex Data Embeddings

We constructed two more complex data cases by i) superimposing instances of 'Trousers' and 'Dress' with MNIST and ii) instances of 'Sandal' and 'Sneaker' with MNIST. Figures 4(a)-4(c) show complex data embeddings with 'Trousers'-'Dress' as Fashion MNIST ground truth labels, while Figures 4(d)-4(f) with 'Sandal'-'Sneaker'. IMAPCE, in both experiments, computes embeddings that provide some separation according to their Fashion-MNIST classes, revealing the complementary structure. On the other hand, cPCA and especially ct-SNE embeddings are highly mixed in terms of their Fashion-MNIST classes.

The test-set accuracies of the trained SVM classifiers for each complex data case are averaged over 10 random train-test splits and provided in Table 3. The very poor performance of the ct-SNE embeddings as well as the superior performance achieved by the IMAPCE ones confirm our observations.

Method	Trouser-Dress	Sandal-Sneaker
cPCA	0.68 ± 0.007	0.75 ± 0.006
ct-SNE	0.10 ± 0.006	0.10 ± 0.005
IMAPCE	$\mathbf{0.86} \pm 0.005$	$\mathbf{0.8} \pm 0.007$

Table 3: Accuracy scores for SVM classification on the 2D embeddings of IMAPCE, cPCA and ct-SNE.

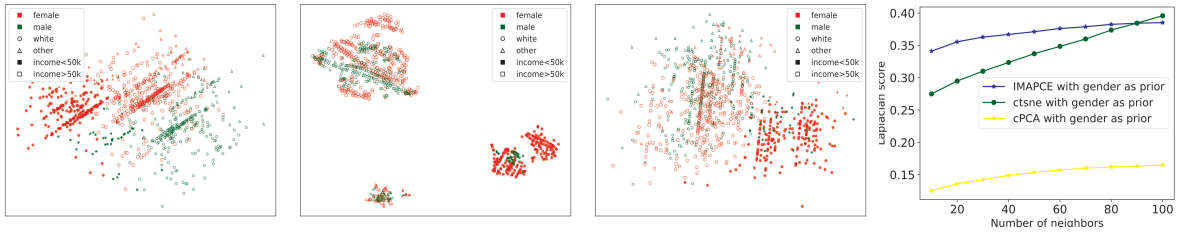

(a) cPCA on synthetic (b) ct-SNE on synthetic (c) IMAPCE on synthetic (d) Laplacian scores

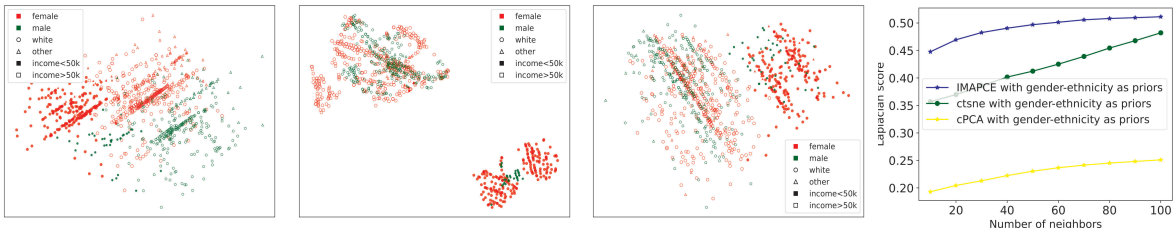

(e) cPCA on adult (f) ct-SNE on adult (g) IMAPCE on adult (h) Laplacian scores

Figure 3: Visualisations of UCI adult data projections computed by cPCA, ct-SNE and IMAPCE and their Laplacian scores. (a), (b), (c) were computed using the gender attribute as prior. (e), (f), (g) were computed using the combination of gender and ethnicity attributes as prior.

D Iterative Exploration of MNIST

We performed the iterative visual exploration of 10000 MNIST instances using both IMAPCE and cPCA. We ran multiple experiments assuming no prior data as well as prior data coming from every ground truth class. Quantitative results are shown in Table 4. IMAPCE outperforms cPCA with respect to both Jaccard and NMI under every prior data assumption.

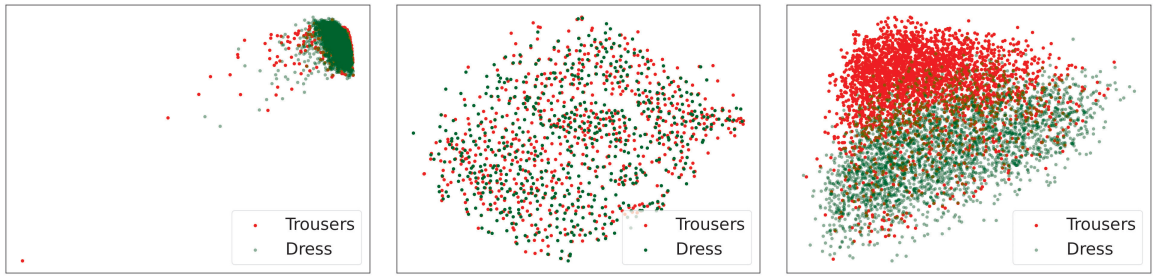

(a) cPCA embeddings (b) ct-SNE embeddings (c) IMAPCE embeddings

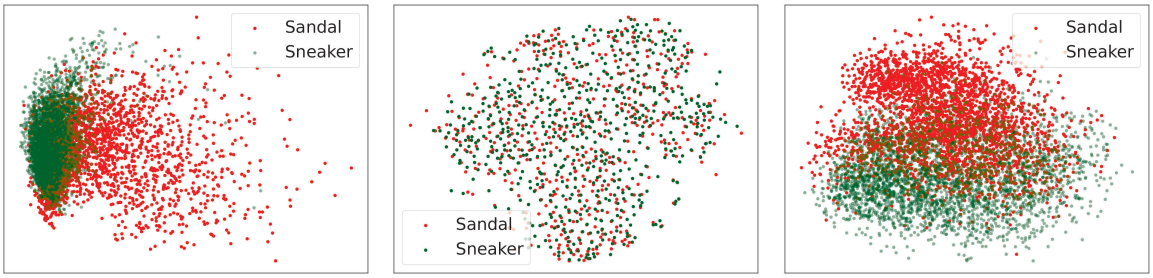

(d) cPCA embeddings (e) ct-SNE embeddings (f) IMAPCE embeddings

Figure 4: Complex data embeddings. (a), (b), (c) for 'Trousers'-'Dress' complex data case and (d), (e), (f) for 'Sandal'-'Sneaker' complex data.

Method	Prior data class	Mean Jaccard score	NMI
IMAPCE	-	$\mathbf{0.41} \pm 0.01$	$\mathbf{0.41} \pm 0.02$
cPCA	-	0.3	0.22
IMAPCE	0	$\mathbf{0.38} \pm 0.01$	$\mathbf{0.39} \pm 0.03$
original cPCA	0	0.21	0.14
IMAPCE	1	$\mathbf{0.33} \pm 0.02$	$\mathbf{0.35} \pm 0.02$
original cPCA	1	0.16	0.09
IMAPCE	2	$\mathbf{0.37} \pm 0.03$	$\mathbf{0.38} \pm 0.02$
cPCA	2	0.31	0.22
IMAPCE	3	$\mathbf{0.34} \pm 0.02$	$\mathbf{0.39} \pm 0.01$
cPCA	3	0.25	0.19
IMAPCE	4	$\mathbf{0.44} \pm 0.03$	$\mathbf{0.42} \pm 0.03$
cPCA	4	0.27	0.19
IMAPCE	5	$\mathbf{0.43} \pm 0.03$	$\mathbf{0.43} \pm 0.02$
cPCA	5	0.26	0.28
IMAPCE	6	$\mathbf{0.32} \pm 0.02$	$\mathbf{0.35} \pm 0.02$
cPCA	6	0.26	0.2
IMAPCE	7	$\mathbf{0.4} \pm 0.03$	$\mathbf{0.38} \pm 0.02$
cPCA	7	0.24	0.2
IMAPCE	8	$\mathbf{0.41} \pm 0.03$	$\mathbf{0.41} \pm 0.03$
cPCA	8	0.27	0.19
IMAPCE	9	$\mathbf{0.42} \pm 0.03$	$\mathbf{0.39} \pm 0.04$
cPCA	9	0.27	0.19

Table 4: Jaccard (averaged over all classes) and NMI scores for evaluation of IMAPCE and cPCA on the exploration of 10000 MNIST samples. Ten different random initializations were used for IMAPCE.